

## Scattering potentials at Si-Ge and Sn-Ge impurity dimers on Ge(001) studied by scanning tunneling microscopy and *ab initio* calculations

Kota Tomatsu, Masamichi Yamada, Kan Nakatsuji, and Fumio Komori\*

*Institute for Solid State Physics, The University of Tokyo, 5-1-5, Kashiwanoha, Kashiwa-shi, Chiba 277-8581, Japan*

Binghai Yan

*Center for Advanced Study, Tsinghua University, Beijing 100084, People's Republic of China*

Chenchen Wang, Gang Zhou, and Wenhui Duan

*Department of Physics, Tsinghua University, Beijing 100084, People's Republic of China*

(Received 24 June 2008; published 4 August 2008)

Scattering potentials for  $\pi^*$  electrons at Si-Ge and Sn-Ge dimers on a Ge(001) surface are studied by scanning tunneling microscopy and *ab initio* calculations. Phase-shift analysis of standing waves in  $dI/dV$  images reveals that Si and Sn atoms located in the conduction path of  $\pi^*$  electrons form potentials with the sign opposite to each other. Density-functional calculations and simple calculations based on the nearly-free-electron model explain the observed potential structures. These results are qualitatively understood by relative  $p$ -orbital energy of the Si, Sn, and Ge atoms.

DOI: [10.1103/PhysRevB.78.081401](https://doi.org/10.1103/PhysRevB.78.081401)

PACS number(s): 73.20.Hb, 68.37.Ef, 82.20.Wt

In recent years, electron transport through atomic-scale wires and molecules has attracted much interest both experimentally and theoretically, especially for possible application to functional devices. So far, conductance of such systems bridged between two electrodes has mainly been studied for this purpose.<sup>1,2</sup> In this approach, transmission at the contact between the system and the electrodes usually dominates the intrinsic conduction. Consequently, it has been difficult to discuss how the local chemical bond in the system influences on the conduction. On the other hand, an approach using one-dimensional (1D) electronic systems at surfaces enables us to study simultaneously the microscopic structure and electron transport by observing topographic images and electronic standing waves in differential conductance ( $dI/dV$ ) images with scanning tunneling microscopy (STM).<sup>3-5</sup> The scattering potential can be also estimated by phase shifts of these waves.<sup>4-6</sup>

Recently, electron scattering by impurity Sn atoms incorporated in a quasi-1D electronic system was studied on the clean Ge(001) surface, where Ge atoms form buckled dimers with  $\pi$  and  $\sigma$  bonds.<sup>7</sup> The dimers line up and make a dimer row, and the neighboring dimers buckle alternately.<sup>8</sup> The  $\pi^*$  electron localizing at the lower atom of the dimer behaves like a 1D electron along the dimer row.<sup>9</sup> A standing wave of the  $\pi^*$  electrons made by a buckled Sn-Ge impurity dimer having its Sn atom at the lower-atom position, “Sn  $L$  dimer,” was observed in the  $dI/dV$  image. Whereas a standing wave by a Sn-Ge dimer having its Sn atom at the upper-atom position, “Sn  $U$  dimer,” was too small to be observed. These results were qualitatively understood by the fact that the  $\pi^*$  electrons propagate on the impurity Sn and host Ge atoms at the Sn  $L$  and  $U$  dimers, respectively.<sup>7</sup> However, the details of the scattering, such as the sign of the scattering potential at the Sn-Ge dimers, have not been clarified.

In the present Rapid Communication, we show standing waves around oppositely-buckled Si-Ge dimers on Ge(001), and discuss the difference in electron scattering between the

Si-Ge and Sn-Ge dimers. The Si, Ge, and Sn belong to group-IV elements, and the energy of their atomic  $p$  orbitals, which form the  $\pi^*$  states, becomes high in order of their atomic number; Si, Ge, and Sn.<sup>10</sup> We found that the Sn and Si atoms in the conduction path form potentials with the sign opposite to each other for the  $\pi^*$  electrons. The sign and amplitude of the scattering potentials qualitatively agree with the results by density-functional calculations and by simple and novel calculations based on the nearly-free-electron model. The difference of the potential structure is explained by the relative  $p$ -orbital energy. Furthermore, we can change the sign of the potential by flipping the buckling orientation of the Si-Ge dimer.

The Ge surface was cleaned by repeating Ar<sup>+</sup> sputtering and annealing up to 1000 K. Silicon and tin atoms were deposited onto the Ge substrate at room temperature from a Si(111) wafer heated at 1300 K and a Sn crucible, respectively. Total coverage of the Si and Sn atoms was less than 5% of the surface atoms. The STM images were obtained at 80 K in an ultrahigh vacuum less than  $1 \times 10^{-9}$  Pa. The  $dI/dV$  images were acquired using a lock-in method with the 30 mV (peak to peak) modulation of the sample bias voltage at 2.8 kHz. The dc current feedback loop was turned on during the scan.

Density-functional calculations were performed within the local-density approximation using the VIENNA *ab initio* simulation package.<sup>11</sup> We used projector augmented wave potentials<sup>12</sup> to describe the core electrons and an energy cut-off of 312.5 eV to expand the wave functions. A repeated-slab model was adopted with 10 Ge layers separated by a 1.3 nm vacuum, and the bottom Ge layer was passivated by H atoms. The Ge atoms on the two bottom layers were fixed, and all the other atoms were fully relaxed until the forces were less than 0.01 eV/Å. Integration over the Brillouin zone was done using Monkhorst-Pack scheme<sup>13</sup> with  $5 \times 7$  k points for the electronic structure calculation.

First, we address adsorption sites of the Si atoms on the

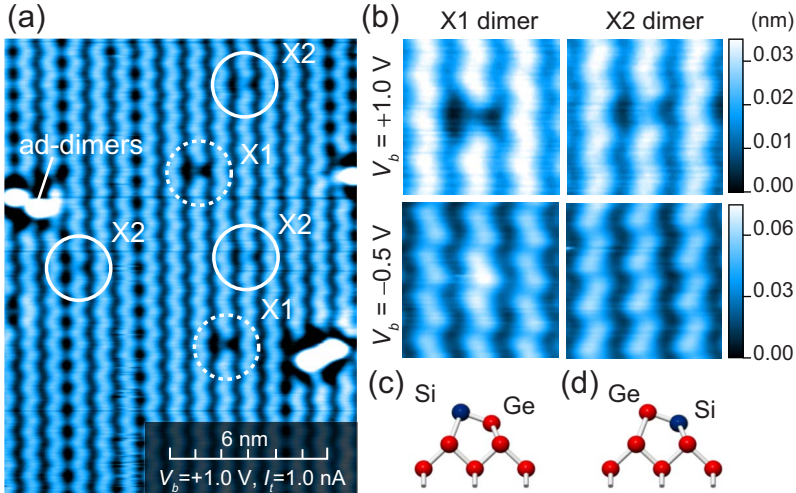


FIG. 1. (Color online) (a) Empty-state image of a Si-deposited Ge(001) surface at 80 K. (b) Bias-voltage dependence of the same X1 and X2 dimers ( $I_t$  is commonly 1.0 nA). (c),(d) Structural models (side view) of the X1 and X2 dimers, respectively.

Ge surface from topographic images. An empty-state image (the sample bias voltage  $V_b = +1.0$  V, and the tunneling current  $I_t = 1.0$  nA) of the Si-deposited Ge(001) surface is shown in Fig. 1(a). In addition to ad-dimers,<sup>14</sup> we notice two kinds of Si-associated dimers at the surface Ge dimer positions as indicated by X1 and X2 in the image. Figure 1(b) shows their bias voltage dependence. Here, it is noted, on the clean surface, the lower (upper) atoms of the buckled Ge dimers are imaged as protrusions in the empty-state (filled-state) image.<sup>8</sup> In the empty-state image ( $V_b = +1.0$  V), the lower atoms of both X1 and X2 dimers are imaged lower than those of the Ge dimers, and the lower atom of the X1 dimer is imaged lower than that of the X2 dimer. On the other hand, in the filled-state image ( $V_b = -0.5$  V), the upper atom of the X1 dimer is imaged higher than those of the Ge dimers, and the X2 dimer is indistinguishable from the Ge dimers.

The buckling orientation of the X1 and X2 dimers can be flipped by changing  $V_b$  at 80 K, and the X1 dimer changes into the X2 dimer vice versa. This indicates that the X1 and X2 dimers are oppositely-buckled Si-Ge dimers. If they are pure Si dimers, the STM image should be the same irrespectively of their buckling orientation. Then, within Tersoff-Hamann scheme,<sup>15</sup> we simulated topographic images of the Si-Ge dimers having its Si atom at the upper-atom position, “Si *U* dimer,” and that at the lower-atom position, “Si *L* dimer,” whose structure was fully relaxed. The observed topographic image of the X1 (X2) dimer agrees with the simulated image of the Si *U*(*L*) dimer. Thus, the X1 (X2) dimer is assigned to the Si *U*(*L*) dimer as illustrated in Fig. 1(c) [Fig. 1(d)]. Our calculations showed that Si *L* dimer is 0.11 eV energetically more favorable than Si *U* dimer. The dimer-bond length and tilt angle are 2.44 Å and 21.9° (2.40 Å and 17.6°), respectively, for Si *L*(*U*) dimer. These are consistent with previous calculations.<sup>16</sup>

Figures 2(a)–2(c) show  $dI/dV$  images of Ge dimer rows including the Si *L* and *U* dimers at  $V_b = +0.55$  V and cross sections along the dimer row at typical  $V_b$ 's. In Fig. 2(d), cross sections of standing waves around the Sn *L* dimer taken under the same conditions are shown for comparison.<sup>7,17</sup> The standing waves around the Si *L* dimer

are weaker than those around the Sn *L* dimer, and detected only at  $V_b < \sim 0.6$  eV. This means that the Si atom in the conduction pathway scatters the  $\pi^*$  electrons more weakly than the Sn atom. Weak standing waves also appear around the Si *U* dimer. For the Si-Ge dimers, unlike the Sn-Ge dimers, there is no significant difference in the wave amplitude between the two oppositely-buckled configurations.

We next analyze the phase shift of the standing waves to elucidate the scattering potential. Intensity of the  $dI/dV$  signal is approximately proportional to surface local density of states (LDOS). For the 1D electronic system, the intensity  $\alpha$  at distance  $x$  measured from the scattering center is given by the equation

$$\alpha(x) = A \cos(2kx + \phi) \exp(-x/d), \quad (1)$$

where  $A$ ,  $k$ ,  $\phi$ , and  $d$  are amplitude, wave number, phase shift, and decay length of the standing wave, respectively.<sup>5</sup> The factor,  $\exp(-x/d)$ , represents damping of the standing wave due to the energy relaxation and the  $V_b$  modulation for

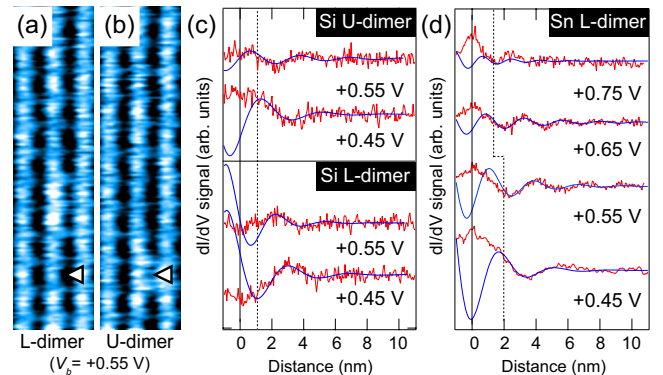


FIG. 2. (Color online) (a),(b)  $dI/dV$  images of Ge dimer rows including the Si *L* and *U* dimers, respectively. The arrows indicate the Si-Ge dimer positions. (c),(d) Line profiles of standing waves around the Si *U* and *L* dimers and those around the Sn *L* dimer at different  $V_b$ 's (Ref. 17). Tunneling current was commonly 1.0 nA. The blue (dark gray) solid curves show the results of fitting Eq. (1) to the data on the right side of the dotted lines.

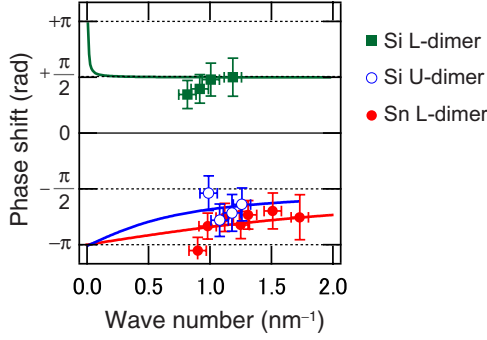


FIG. 3. (Color online) Phase shift of the standing waves around the Si *L*, Si *U*, and Sn *L* dimers in Fig. 2. The solid curves are the results of fitting with Eqs. (2) and (3). For details, see the main text.

the lock-in detection.<sup>18</sup> We obtained the  $\phi$ - $k$  relation by fitting Eq. (1) to the observed standing waves. Here, fitting parameters are  $A$ ,  $\phi$ , and  $d$ , and the value of  $k$  was independently determined from strong standing waves around the steps or the ad-dimers in the same image; the amplitudes of the standing waves around the Si-Ge dimers were so small that fitting with the four independent parameters causes large errors in  $k$  and  $\phi$ . Because of the tip-height change during the measurements on the  $dI/dV$  signal, the observed  $dI/dV$  image does not reflect the actual spatial mapping of LDOS when a tip-surface distance is not constant.<sup>19</sup> Thus, the data at the area close to the Si-Ge (Sn-Ge) dimers, where the tip height largely varies [the left side of the dotted lines in Figs. 2(c) and 2(d)], were not used for the curve fitting. The results are shown as the solid curves in Figs. 2(c) and 2(d), and the obtained  $\phi$ - $k$  relation in Fig. 3. Phase shifts were found to be about  $+0.5\pi$ ,  $-0.6\pi$ ,  $-0.7\pi$  for Si *L*, Si *U*, and Sn *L* dimers, respectively, and almost constant for  $1.0 \text{ nm}^{-1} < k < 1.8 \text{ nm}^{-1}$ .

We now compare the obtained  $\phi$ - $k$  relation with those calculated using a rectangular-potential barrier or well. For the potential barrier, the  $\phi$ - $k$  relation is given by

$$\phi(k; W, H) = \arg\left(\frac{k^2 + \beta^2}{k^2 - \beta^2 + 2ik\beta \coth \beta W}\right) - kW, \quad (2)$$

and for the potential well, it is given by

$$\phi(k; W', H') = \arg\left(\frac{k^2 - \beta'^2}{k^2 + \beta'^2 + 2ik\beta' \cot \beta' W'}\right) - kW', \quad (3)$$

where  $\beta = \sqrt{2m^*H/\hbar^2 - k^2}$  and  $\beta' = \sqrt{2m^*H'/\hbar^2 + k^2}$ . The parameters  $W$  ( $W'$ ) and  $H$  ( $H'$ ) are width and height (depth) of the barrier (well), respectively, and  $m^*$  is the effective mass of the  $\pi^*$  electron. Here, we fixed  $W$  and  $W'$  to one dimer separation (0.40 nm) because the  $\pi^*$  electrons are scattered by a single dimer. For  $m^*$ , we adopted the value,  $0.15 m_0$  ( $m_0$ ; free-electron mass), which was obtained in our band calculation. The height  $H$  ( $>0$ ) or depth  $H'$  ( $>0$ ) at the Si-Ge and Sn-Ge dimers were determined by fitting Eqs. (2) and (3) to the  $\phi$ - $k$  relation in Fig. 3. The results are shown by the solid curves in Fig. 3. We obtained potential barriers of 0.4–1.2 eV and 1.3–2.5 eV for Si *U* and Sn *L* dimers, respectively, and a potential well of 0–0.4 eV for the Si *L* dimer. Interestingly, the Si and Sn atoms located in the conduction pathway (i.e., the Si and Sn *L* dimers) form potentials with the opposite signs. Reflection coefficients calculated from the obtained rectangular potentials are 40%–70%, 10%–40%, 0%–10% for Sn *L*, Si *U*, and Si *L* dimers, respectively, at  $k = 1.2 \text{ nm}^{-1}$ .

These experimentally-obtained scattering potentials have been examined by *ab initio* calculations. We calculated the electronic state of a supercell composed of four Ge- $p(2 \times 2)$  unit cells with one impurity (Si-Ge or Sn-Ge) dimer as illustrated in Fig. 4(a). Figures 4(b) and 4(c) show the energy dispersion of the  $\pi^*$  band along the dimer row ( $\bar{\Gamma}$  to  $\bar{J}'$ ) in the extended Brillouin-zone scheme for the Si and Sn *L* dimers, respectively. At the first Brillouin-zone (FBZ) boundary ( $k = \pi/l$ , where  $l$  is the superlattice constant along the dimer row, 3.19 nm), the  $\pi^*$  band splits by 0.012 (0.04) eV for the Si(Sn)*L* dimer because the impurity dimer brings a periodical potential  $V(x)$  to the original quasi-1D system along the dimer row.

In the nearly-free-electron model, the gap energy  $\Delta E$  is given by

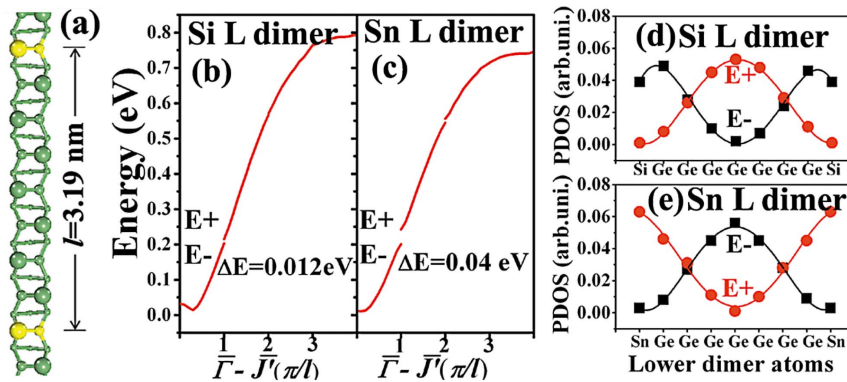


FIG. 4. (Color online) (a) Unit cell utilized for the calculation. The red (gray) and yellow (light gray) dimers stand for the Ge and impurity (Si-Ge or Sn-Ge) dimers. (b),(c) Energy dispersion of the  $\pi^*$  band in the extended Brillouin zone for the dimer row with the Si and Sn *L* dimers, respectively. (d),(e) Projected density of states at  $E_{\pm}$  to the lower-dimer atoms along the dimer row with the Si and Sn *L* dimers, respectively. The solid red (gray) circles and black squares represent  $E_+$  and  $E_-$  states, respectively, with the solid lines for eye guide.

$$\Delta E = 2|V(G)| = 2 \left| \frac{1}{l} \int V(x) e^{iGx} dx \right|, \quad (4)$$

where  $G=2\pi/l$  is the reciprocal-lattice vector.<sup>20</sup> For a rectangular potential,  $|V(G)|$  is given by

$$|V(G)| = \frac{1}{\pi} |U| \sin(\pi W/l), \quad (5)$$

where  $U$  is the height or depth of the potential;  $U>0$  ( $U<0$ ) for the potential barrier (well). Using Eqs. (4) and (5), we obtain  $|U|=0.05(0.16)$  eV for the Si(Sn) $L$  dimer at  $W=0.40$  nm.

For the potential well, the lower (higher) energy state at the FBZ boundary,  $E_-$  ( $E_+$ ), has a charge-density maximum (minimum) around the impurity dimers. For the potential barrier, the relation is opposite. Figures 4(d) and 4(e) show the charge density of the  $E_{\pm}$  states projected to the lower-dimer atoms along the dimer row for the Si and Sn  $L$  dimers, respectively. We notice that, around the Si(Sn) $L$  dimer, the charge density of the  $E_-$  state has a maximum (minimum) and that of the  $E_+$  state has a minimum (maximum). Thus, we conclude that a potential well (barrier) with  $U=-0.05$  ( $+0.16$ ) eV is formed at the Si(Sn) $L$  dimer. With the same method, we obtain  $\Delta E=0.012$  eV and  $U=+0.05$  eV for the Si  $U$  dimer, and  $\Delta E=0.02$  eV and  $U=+0.08$  eV for the Sn  $U$  dimer. These values are consistent with the following experimental results; (1) the potential due to the Si  $L$  dimer has negative sign and those due to the Si  $U$  and Sn  $L$  dimer

have positive one. (2) the scattering amplitude by the Sn  $L$  dimer is the largest among the four impurity dimers.

The difference of the potential between the Sn and Si  $L$  dimers can be qualitatively understood by the relative  $p$ -orbital energy of Si, Ge, and Sn atoms. The  $\pi^*$  state consists mainly of the  $p$  orbitals of the lower-dimer atom,<sup>8</sup> and the  $p$ -orbital energy increases in order of the atomic number; Si ( $-4.17$  eV), Ge ( $-4.08$  eV), and Sn ( $-3.93$  eV).<sup>10</sup> Since the  $p$ -orbital energy of Ge is higher than that of Si, a potential well will be formed at the Si  $L$  dimer. Whereas, the Sn  $L$  dimer forms a potential barrier because the  $p$ -orbital energy of Sn is higher than that of Ge. The difference in the  $p$ -orbital energy between the Ge and Sn atoms is larger than that between Ge and Si atoms. This may result in the stronger scattering at the Sn  $L$  dimer than at the Si  $L$  dimer.

Our calculations qualitatively account for the experimental results. However, the absolute values of the potential height and depth are different from the corresponding experimental results. This discrepancy can be attributed to our simple assumptions such as 1D free-electron-like energy dispersion of the  $\pi^*$  state and a rectangular-potential model. Experimentally, tip-induced band bending<sup>21</sup> causes a considerable error in the observed  $k$ , and hence in the phase-shift analysis. Further theoretical investigations as well as more quantitative measurements for the electronic states are needed for solving it.

The authors sincerely thank J. Ihm and M. Tsukada for their valuable comments. This work has been partially supported by JSPS-NSFC-KOSEF, A3 Foresight Program.

\*komori@issp.u-tokyo.ac.jp

<sup>1</sup>A. H. Flood, J. F. Stoddart, D. W. Steuerman, and J. R. Heath, *Science* **306**, 2055 (2004)

<sup>2</sup>L. Venkataraman, J. E. Klare, C. Nuckolls, M. S. Hybertsen, and M. L. Steigerwald, *Nature (London)* **442**, 904 (2006).

<sup>3</sup>M. F. Crommie, C. P. Lutz, and D. M. Eigler, *Nature (London)* **363**, 524 (1993).

<sup>4</sup>Y. Hasegawa and Ph. Avouris, *Phys. Rev. Lett.* **71**, 1071 (1993).

<sup>5</sup>Ph. Avouris, I.-W. Ryo, R. E. Walkup, and Y. Hasegawa, *J. Vac. Sci. Technol. B* **12**, 1447 (1994).

<sup>6</sup>T. Yokoyama, M. Okamoto, and K. Takayanagi, *Phys. Rev. Lett.* **81**, 3423 (1998).

<sup>7</sup>K. Tomatsu, K. Nakatsuji, T. Iimori, Y. Takagi, H. Kusunohara, A. Ishii, and F. Komori, *Science* **315**, 1696 (2007).

<sup>8</sup>M. Needels, M. C. Payne, and J. D. Joannopoulos, *Phys. Rev. B* **38**, 5543 (1988).

<sup>9</sup>K. Nakatsuji, Y. Takagi, F. Komori, H. Kusunohara, and A. Ishii, *Phys. Rev. B* **72**, 241308(R) (2005).

<sup>10</sup>S. Kotochigova, Z. H. Levine, E. L. Shirley, M. D. Stiles, and C. W. Clark, *Atomic Reference Data for Electronic Structure Cal-*

*culations*, version 1.4 (National Institute of Standards and Technology, Gaithersburg, MD, 2005).

<sup>11</sup>G. Kresse and J. Hafner, *Phys. Rev. B* **47**, 558(R) (1993); G. Kresse and J. Furthmuller, *ibid.* **54**, 11169 (1996).

<sup>12</sup>G. Kresse and D. Joubert, *Phys. Rev. B* **59**, 1758 (1999).

<sup>13</sup>H. J. Monkhorst and J. D. Pack, *Phys. Rev. B* **13**, 5188 (1976).

<sup>14</sup>W. Wulfhekel, B. J. Hattink, H. J. W. Zandvliet, G. Rosenfeld, and B. Poelsema, *Phys. Rev. Lett.* **79**, 2494 (1997).

<sup>15</sup>J. Tersoff and D. R. Hamann, *Phys. Rev. B* **31**, 805 (1985).

<sup>16</sup>S. C. A. Gay and G. P. Srivastava, *Phys. Rev. B* **60**, 1488 (1999).

<sup>17</sup>The sign of  $dI/dV$  signal shown in Ref. 7 was erroneously inverted. The main conclusions are not changed.

<sup>18</sup>L. Burgi, H. Brune, O. Jeandupeux, and K. Kern, *J. Electron Spectrosc. Relat. Phenom.* **109**, 33 (2000).

<sup>19</sup>J. Li, W.-D. Schneider, and R. Berndt, *Phys. Rev. B* **56**, 7656 (1997).

<sup>20</sup>H. Ibach and H. Lüth, *Solid-State Physics: An Introduction to Principles of Materials Science* (Springer-Verlag, Berlin, 1995).

<sup>21</sup>M. McEllistrem, G. Haase, D. Chen, and R. J. Hamers, *Phys. Rev. Lett.* **70**, 2471 (1993).